Field-driven sense elements for chirality-dependent domain wall detection and storage

S. R. Bowden[1,2] and J. Unguris[1]

[1]*Center for Nanoscale Science and Technology, National Institute of Standards and Technology, Gaithersburg, MD 20899*

[2]*Maryland Nanocenter, University of Maryland, College Park, MD 20742*

A method for locally sensing and storing data of transverse domain wall chirality in planar nanowire logic and memory systems is presented. Patterned elements, in close proximity to the nanowires, respond to the asymmetry in the stray field from the domain wall to produce a chirality-dependent response. When a bias field is applied, a stray-field-assisted reversal of the element magnetization results in a reversed remanent state, measurable by scanning electron microscopy with polarization analysis (SEMPA). The elements are designed as triangles with tips pointing toward the nanowire, allowing the shape anisotropy to be dominated by the base but having a portion with lower volume and lower energy barrier closest to the domain wall. Micromagnetic modeling assists in the design of the nanowire-triangle systems and experiments using SEMPA confirm the importance of aspect ratio and spacing given a constant bias field magnitude.

I. INTRODUCTION

The control of domain wall movements and interactions in magnetic nanowires has received considerable interest within the past decade ever since the introduction of novel methods for logic[1-3] and storage[4-6]. This ongoing study of new systems for magnetic computing is expected to yield devices that will have application in niche markets where it is advantageous to combine information processing with data non-volatility and radiation hardness, such as in secure file transfers and smart memories. Further, the energy dissipation is several orders of magnitude lower (due strictly to hysteresis losses) than conventional CMOS devices[7].

Nanomagnetic logic schemes typically function by controlling the magnetization of magnetically soft planar conduits (through controlled domain wall motion[1,8]) or single domain nanomagnets (through magnetostatic interactions[2-3]). Recent work has also concentrated on

utilizing domain walls themselves for functions such as clocking[9] and the assisted switching of magnetic elements[10, 11] by taking advantage of their stray field[12].

In addition to being mobile sources of localized stray field, domain walls may also be exploited as carriers of binary data due to the bistable nature of their internal spin chirality. Walls in the transverse orientation, favored in thinner and narrower nanowires[13], have two stable configurations where the magnetization in its center points toward either edge of the nanowire. Recent experiments have demonstrated chirality-dependent behavior that lead to conditional changes of logic states. These experiments demonstrate the promise of using domain walls as controllable bits in non-volatile logic systems. Chirality-dependent interactions have been observed within nanowires[14,15], between neighboring wires[16, 17], in curved wires[18], and at artificial defects[19].

As with any logic scheme, mechanisms for read-out and data storage are necessary to complete a viable processing system. Nanomagnetic logic offers the opportunity to combine these capabilities with the logic unit itself. In a domain wall chirality-based device, integration is accomplished by locally storing and reading the domain wall structure before further operations and interactions alter its configuration. Bashir et al.[20] presented modeling results on the remote detection of domain wall field, structure, and orientation by creating elliptical elements adjacent to a nanowire. The magnetization of the ellipse is altered by the domain wall stray field and is measured via giant magnetoresistance (GMR). The chirality of a transverse wall is then detected by taking advantage of the asymmetry in the stray field emitted by the domain wall above versus below the nanowire in the pattern plane.

In this paper a method of sensing and locally storing the transverse domain wall chirality is presented by placing a pair of triangular elements, one above and one below, adjacent to the nanowire in the sample plane of a single layer Permalloy (Py), $Ni_{81}Fe_{19}$, system (Fig. 1a). In addition to measuring chirality, these structures are also designed to allow non-volatile storage of this information, allowing a measurement pulse to be made at any time after the domain wall has passed through the wire. By utilizing these elements as the free layer in a GMR stack, integrated sensing and storage of transverse domain wall information may be achieved. Since the triangle elements are larger than the domain wall, a gain in the GMR ratio is achieved relative to measuring the domain wall orientation by simply passing current perpendicular to the plane through a portion of the nanowire itself. Additionally, measuring the GMR off-wire frees up complexities in fabrication and allows the domain wall to pass through the sensor relatively unimpeded.

In Section II the operation and design methodology of this system is described. In Section III results from simulations using OOMMF (the Object Oriented MicroMagnetic Framework)[21] are detailed, which were performed to study the domain wall-assisted reversal of triangles as well as to create phase diagrams of the triangle response. Results from experimental systems are described in Section IV before concluding remarks are made in Section V. Scanning electron microscopy with polarization analysis (SEMPA)[22] was used to directly image and characterize the magnetic configuration of the domain walls and triangles in the experiments.

II. EXPERIMENT DESIGN AND METHODOLOGY

Patterned triangles have been studied in the past to test their properties as magnetic storage elements[23-26]. In this case we make use of the buckle state[23,] where there is a net longitudinal (*x* axis) magnetization that curves upward or downward at remanence due to shape anisotropy, as shown in Fig. 1a. This net magnetization is set by applying global field pulses with components along the wire axis. The domain wall is maintained in the transverse regime by keeping the Py nanowire ≤ 150 nm in width and 10 nm in thickness. A field pulse, $\boldsymbol{B}_{\mathrm{p}}$ (shown in Fig. 1a), is applied to the system to move a domain wall from left to right. As it passes the vicinity of a triangle element, the emitted stray field may reorient the spins at the tip of the triangle, which ultimately induces a 180° flip in longitudinal magnetization due to $\boldsymbol{B}_{\mathrm{p}}$. Thus, the choice of using triangles as remote sensing elements becomes apparent: the longitudinal component of magnetization, primarily at the base of the triangle, maintains a switchable remanent state that is measurable by SEMPA and is biased by the same field that propagates the domain wall, while the triangle tip, with relatively lower volume and location close to the nanowire, has a lower energy barrier for reversal and responds to the domain wall stray field, which is ideal for sensing. Relevant parameters for the shape and placement of the triangle elements are shown in Fig. 1a. Parameters include the spacing, *s*, defined as the distance between the triangle tip and the nanowire edge, the triangle base, *b*, and the height, *h*. The aspect ratio, *a*, of a triangle is defined as *b*/*h*. The thickness, *t*, is the same for the nanowire and triangular sensor elements in all simulations and experiments.

The chirality of the domain wall is set by the nucleation field, $\boldsymbol{B}_{\mathrm{n}}$, which acts on the curved nucleation structure similar to previously used methods[11,18]. The curved nucleation structure is shown attached to the straight part of the nanowire in Fig. 1a. The field $\boldsymbol{B}_{\mathrm{n}}$ initializes

the system by magnetizing the nanowire and triangles to the left, while nucleating a head-to-head domain wall in the curvature with chirality oriented in the direction of $\boldsymbol{B}_n$. The direction of $\boldsymbol{B}_n$ is slightly angled towards the nanowire such that when the propagation field, $\boldsymbol{B}_p$, is applied in the longitudinal direction, the domain wall travels through the nanowire instead of annihilating at the opposite end of the curved part of the conduit. A domain wall with opposite chirality is produced when the nucleation structure curves in the opposite direction. Thus, the curved structure allows the setting of domain wall chirality, the initialization of the elements, the propagation of the domain wall, and the biasing of the elements to be carried out simultaneously using only longitudinal field pulses.

The state of the magnetic patterns in Fig. 1a shows the expected, correct configuration after a head-to-head domain wall with an upward oriented chirality passes the triangle pair. Only the upper triangle has reversed its longitudinal magnetization from left to right due to the domain wall orientation, while the lower triangle maintains a magnetization in the $-x$ direction.

The OOMMF calculation of the stray field emitted by a transverse domain wall in Fig. 1c illustrates the reason for this expected behavior. The stray field is calculated from a Py nanowire[27] 10 nm thick and 100 nm wide, the same geometry studied in the experimental results to follow. Fig. 1b shows the transverse magnetic stray field, B_y, along the line at $x = 0$ which approximately bisects the domain wall, while Fig. 1c shows horizontal line scans of B_y at the two different spacings both above and below the nanowire. Above the nanowire B_y maintains a positive sign and decreasing magnitude. Below the nanowire B_y first has a positive sign, dominated by the transverse domain wall direction, and then changes to a negative sign, reaching a minimum of -6.13 mT before decreasing in magnitude. The negative sign of B_y below

the nanowire is consistent with the diverging monopolar nature of the two head-to-head domains that form the domain wall. Thus, in the plane of the nanowire, the stray field from the domain wall is a combination of a dipole-like term from the transverse oriented spins and a monopole-like term from the head-to-head domains as discussed by Hayward et al.[17] and Bashir et al.[20] As seen in the bottom panel of Fig. 1c, a spacing of 5 nm leads to relatively high fields and a high asymmetry. B_y reaches a maximum of +320 mT above the nanowire due to the additive nature of the monopolar and dipolar terms. This is compared to a value of +53 mT at the same position but 5 nm below the nanowire. A maximum asymmetry in B_y ($B_{y,+s}(x) - B_{y,-s}(x)$) of 272 mT occurs at x = -10 nm. At a larger spacing of 35 nm, where fabrication tolerances are more practical, there is a still significant maximum field difference of 59 mT (top panel of Fig. 1c). The design of the sensors will therefore be sensitive to their spacing from the nanowire.

When a triangle pair's geometry and spacing is properly designed, a triangle placed on the side of the nanowire with stronger stray field will change the sign of its longitudinal magnetization, while the triangle on the opposite side will not. The spins at the tip of the triangle on the side with stronger field will momentarily reorient to the transverse direction. This then initiates a complete reversal of the longitudinal magnetization to the direction of $\boldsymbol{B}_p$. If the same properly designed and spaced triangle is mirrored onto the side of the nanowire with weaker field, the triangle will not undergo a change in longitudinal magnetization as it is less aided by the stray field. In the case of head-to-head transverse domain walls, an upward pointing chirality should switch only an element placed above the nanowire while a downward chirality should switch only an element below. Placing a pair of triangles on either side of a nanowire allows detection of not only domain wall chirality but also whether or not a domain

wall has traversed that point of the nanowire. When $\boldsymbol{B}_p$ is reduced to zero, the sign of the longitudinal magnetization is maintained in the remanent state. Such a properly designed system allows measurement of the chirality in zero-field conditions even after the domain wall has propagated out of the nanowire.

III. MICROMAGNETIC MODELING

To aid in the proper design described in Section II and to gain an understanding of the interaction between a domain wall and a sensor pair, micromagnetic simulations using OOMMF were performed. The pinning field created by the triangle pair has implications on device speed and is characterized and compared to previously designed elliptical sensors in Section IIIa. Section IIIb shows implications from scaling on sensor performance and demonstrates the upper and lower limits on triangle size. In Section IIIc phase diagrams of triangle behavior are compiled to aid in experimental designs.

a. Domain Wall Pinning Field

As a domain wall propagates past an adjacent element, it will encounter pinning as a result of magnetostatic interactions between it and the element that will slow the movement of data through the system. One way to quantify the degree of this slowing is to calculate the minimum field that must be applied to free a completely pinned domain wall. Therefore, the depinning field, B_D, of a Py triangle pair was modeled[28]. Triangles with a geometry of b = 900 nm, a = 1.406, and t = 10 nm at a spacing of 40 nm, along with a nanowire 100 nm wide, were first initialized in the $-x$ direction. After reaching its remanent state, a domain wall was injected into the nanowire by applying $\boldsymbol{B}_p$ in the $+x$ direction. The field was then reduced to zero just before the domain wall reached the triangle pair. $\boldsymbol{B}_p$ was then reapplied in increments of 0.5 mT

until the domain wall depinned at B_D = 6.5 mT. For reference, B_D was also calculated for circular elements similar to the scheme described by Bashir et al.[20] to test if a stronger diverging field from the triangle tip produces a larger degree of pinning. A pair of circles with the same area and position as the triangles (radius of 302.8 nm) yielded a pinning field of B_D = 9.5 mT, while a pair of circles with the same height and position as the triangles (radius of 391.3 nm) yielded B_D = 8.5 mT. The domain wall passes the triangle pair when they are set in a buckle state, with a net longitudinal magnetization, and leads to a pinning field that is less than the circular structures' at a spacing of 40 nm, thus avoiding a large field gradient and steeper potential barrier.

b. Triangle Element Scaling

OOMMF simulations were also carried out in order to study the effects of triangle geometry and scaling on the switching mechanism and overall performance of the sensing elements. The results in Fig. 2 exemplify some of the relevant issues when designing triangle sense elements. The results show the switching behavior of three triangle pairs, all with the same designed aspect ratio of 1.163 but varying overall sizes. The value of *b* is equal to 284 nm for the left pair (triangles 1 and 2), 426 nm for the middle pair (triangles 3 and 4), and 560 nm for the right pair (triangles 5 and 6). Fig. 2a shows three frames of the simulation results where a domain wall with an upward chirality is moved from left to right through a Py nanowire 150 nm wide[29]. The structures were first initialized in the –*x* direction and allowed to reach their remanent state. The field was then increased in increments of 0.5 mT in the +*x* direction until the domain wall depinned from the nucleation structure at 14.5 mT. The magnetic orientation just before the domain wall enters into the vicinity of the leftmost pair is shown in Fig. 2a(i).

Here, we see the case that the propagation field of $\boldsymbol{B}_p$ = 14.5 mT is greater than the coercive field for triangle 6 (12.5 mT) and the longitudinal component of magnetization has spontaneously reversed to the +*x* direction before ever being influenced by the domain wall. For the smallest pair, triangles 1 and 2, the balance between shape and exchange anisotropy results in a significant transverse magnetization component in the –*y* direction. Without a relatively extensive base length, the horizontally aligned spins at the base cannot maintain the buckle state through the exchange interaction. Instead, the increased transverse shape anisotropy at the triangle tip dominates the entire triangle magnetization. The middle pair maintains the desired initialized state at the time the bias field is applied. Thus, for the particular system described here with $\boldsymbol{B}_p$ = 14.4 mT, the optimum range for the triangle base is somewhere within 284 nm < *b* < 560 nm.

The next two frames of the simulation, shown in Figs. 2a(ii) and 2a(iii), demonstrate the switching mechanism of the elements in response to the domain wall. The larger transverse field above the nanowire is enough to begin the switching process. Starting at the triangle tip, the spins orient in the same direction as the domain wall stray field. This reorientation, which originates at the tip, then propagates toward the base as it is aided by the bias field, as seen with triangle 3 in Fig. 2a(ii). The bottom triangle in the middle pair, triangle 4, has an insignificant response to the domain wall due to the weak stray field on that side of the nanowire. In Fig. 2a(iii) triangle 3 has completed its switching in the direction of $\boldsymbol{B}_p$, whereas the domain wall has also begun the same switching process in triangle 5. Triangle 5, with the same geometry as triangle 6, correctly switches as a result of the domain wall orientation, even though triangle 6 has incorrectly switched spontaneously. It is also worth noting that the

domain wall and the bias field $\boldsymbol{B}_p$ have had little impact on the state of the first pair. Triangle 1 remains fixed in a transverse orientation.

The switching process of the elements shown from the simulation in Fig. 2a is further illustrated in Fig. 2b. The figure shows the normalized longitudinal magnetization and transverse magnetization of each triangle as a function of domain wall position. The domain wall position is taken as the point along the nanowire length where the transverse magnetization is at a maximum 54 nm down from the top edge of the nanowire. The domain wall position scale is shown at the bottom of Fig. 2a. The top row of graphs in Fig. 2b shows the changes in the two in-plane magnetization components for the upper triangles, while the bottom row shows the paired elements below the nanowire. For the first pair of elements, the response to the domain wall is virtually identical with no change in the sign of M_x. The middle pair exhibits the correct behavior for a sensor design and shows triangle 3 changing the sign of M_x as soon as the domain wall position reaches the vicinity of the triangle edge.

For the larger sized element, triangle 5, there is a longer switching time compared to the smaller triangle 3. As the spin reorientation propagates from tip to base, there is a peak in M_y in the direction of the domain wall stray field (upper right panel of Fig. 2b) that coincides with the overall change in sign of M_x and occurs when the domain wall is 0.16 μm away from the center of triangle 3, resulting in a switching delay time. In the case of triangle 5, there is a larger delay between when the domain wall reaches the vicinity of the element and when the element has completed switching, owing to its increased size. The peak in M_y doesn't occur until the domain wall is 0.46 μm away from the center of triangle 5. Therefore, with a 72 % increase in size, there was an approximately 188 % increase in the switching delay time (assuming constant domain

wall velocity) between triangles 3 and 5. For the triangles below the nanowire, there is only a slight change of M_y in the $-y$ direction, indicating that at such a close spacing, the triangle tips are dominated by the negative-going monopolar component of the stray field.

c. Phase Diagrams of Triangle Response

While the results in Fig. 2 demonstrate the implications of overall element size given a fixed aspect ratio and field amplitude, to get a truer sense of the design space, phase diagrams of expected results were developed using OOMMF. This was done to aid in the design of experimental systems, which were then compared to the modeling results.

The pattern design and modeling conditions used to create the phase diagrams follow. The Py patterns have the design shown in Fig. 1a, with the exception that the curved nucleation structure extends over the top side of the nanowire to nucleate domain walls with downward chirality. A single triangle pair is placed 2.4 μm away from the point where the straight and curved part of the nanowire meet. For all phase diagram simulations and experiments, the nanowire width is 100 nm, the thickness is 10 nm, and the radius of curvature of the nucleation structure is r = 600 nm. The nanowire is first completely magnetized at 68.2° from the $-x$ direction while the triangles are completely magnetized in the $-x$ direction. Through energy minimization[30], the initial remanent state of the system is calculated, which includes the triangles in leftward buckle states and the nanowire with a downward oriented head-to-head domain wall at the bottom of the nucleation structure. The minimum propagation field of 7.5 mT was applied to the initial remanent state using a Runge-Kutta method to solve the Landau-Lifshitz-Gilbert equation[31]. At propagation fields higher than the Walker field, a moving domain wall may undergo spontaneous and periodic chirality reversals[32], and this Walker breakdown

behavior was never observed in the modeling using fields of this magnitude. For these calculations for the phase diagrams, a routine was used to correct for jagged pixelation errors. Once the domain wall has propagated to the right side of the nanowire, the final remanent state is calculated, and the total longitudinal magnetization component of each cell in an element is summed. After analyzing each element, one of the four outcomes outlined in Fig 3a results: “no switch” if neither element switches their magnetization to the right, “correct” if only the bottom element switches, “incorrect” if only the top element switches, and “both switch” if both elements switch.

The phase diagrams developed in Fig. 3b show triangle behavior indicated by coloring. Shading indicates possible phase boundaries given the data points created by the simulations. Successful designs are indicated by the green coloring for two different applied fields (7.5 mT and 10 mT). The parameters comprise four aspect ratios (1.155, 1.406, 1.711, and 2.105), two spacings (10 nm and 40 nm), and five base lengths (300 nm, 600 nm, 900 nm, 1200 nm, and 1500 nm). While a spacing of 40 nm is easily within fabrication limits, a value of 10 nm was studied to determine if an advantage exits in having a tighter spacing specification. The colored shading corresponds with the 40 nm element spacing (open circles). The dotted green line corresponds to the 10 nm element spacing (filled dots) and represents the extension of the correct phase to include higher aspect ratios and triangle sizes with a closer spacing. There were also no incorrect results from these simulations, demonstrating robust chirality detection in the correct phase space and no spontaneous chirality reversals in the > 2 μm distance the domain wall travels to the triangle pair.

The results in Fig. 3b(i) for the applied field of 7.5 mT show that, in general, there is a tight range of aspect ratios that yield the correct result. From the parameters chosen, only the aspect ratio of 1.406 yields the correct results for a spacing of 40 nm. The importance of aspect ratio comes from achieving the ideal level of longitudinal shape anisotropy. A high aspect ratio triangle, with higher anisotropy has an increased coercivity and resists a reversal in the direction of the applied field even under the influence of the domain wall's stray field. A low aspect ratio element has lower coercivity and thus both triangles may switch spontaneously in the presence of the $\boldsymbol{B}_p$. A closer spacing of 10 nm results in an additional correct data point at a higher aspect ratio of 1.711, indicating that at this spacing, the stray field of the domain wall is strong enough to reorient the spins in a larger portion of the triangle. The increased transverse component then lowers the field necessary to induce a longitudinal reversal and the element switches.

At the higher propagation field, Fig. 3b(ii), there is also a tight specification for aspect ratio but with a reduction in the correct phase for the 40 nm spacing. This is due to the applied field becoming greater than the coercivity of the larger-sized triangles and switching both elements in the pair. There is an increase in the design space for the 10 nm spacing to include aspect ratios of 1.711 and 2.105, as seen with the dotted line in Fig. 3b(ii). With an increased value of $\boldsymbol{B}_p$, the smaller spacing accommodates higher aspect ratios and base lengths due to the combination of higher domain wall stray field and higher bias field. The higher domain wall stray field again influences a larger portion of the triangles, and the larger bias is enough to switch the geometries with high coercivity and high aspect ratio. Thus, the design space and scalability of these elements are strong functions of the aspect ratio and the biasing field.

IV. EXPERIMENTAL

Experimental systems were fabricated and characterized to compare to micromagnetic results and identify nanowire and triangle geometries that work reliably together. The experimental patterns had similar designs to those discussed in the micromagnetic results to allow the experiments to be conducted with uniaxial field pulses. A curved nucleation structure with radius r = 600 nm is used in each case, with the wire widths being either 100 nm or 150 nm. For each nanowire studied, two triangle pairs of matching geometry are placed 4.3 μm and 7.7 μm away from the leftmost point of the straight part of the nanowire. The triangles were designed to have ratios of base to isosceles side length of 1, 1.05, 1.1, 1.15, 1.175, 1.2, 1.25, and 1.3, leading to aspect ratios of about 1.155, 1.234, 1.317, 1.406, 1.452, 1.500, 1.601, and 1.711 respectively. The base length designs were 300 nm, 600 nm, 900 nm, 1.2 μm, and 1.5 μm, and the spacings were 40 nm, 70 nm, and 100 nm, encompassing the “no switch”, “correct”, and “both switch” regions of the phase diagrams in Fig. 3b.

The patterns were fabricated on p-doped Si wafer substrates via electron beam lithography using polymethyl methacrylate (PMMA) resist of relative molecular mass 495,000 g/g, electron beam physical vapor deposition, and lift-off. A reactive ion etch was performed after developing with a 1:3 by volume solution of methyl isobutyl ketone to isopropyl alcohol to clean the exposed substrate of resist before Py metallization. The Py was deposited to a thickness of 10 nm, immediately followed by the deposition of a 2 nm Au passivation layer. The maximum error in fabricated structures compared to design was 10 %.

SEMPA measurements were made to image the initial and final magnetization states of the triangles and nanowire system as well as the domain wall structure. This technique allows

direct, quantitative imaging of the surface magnetization with an in-plane resolution of at least 20 nm[22] by analyzing the spin of secondary electrons from a magnetic material. The efficiency of SEMPA's low energy diffuse electron scattering spin analyzers requires a slow scan rate to analyze the magnetic state, thus allowing imaging of only the remanent magnetization state. The sample is kept in an ultra-high vacuum of 3 x 10^{-8} Pa to 10 x 10^{-8} Pa to accommodate the technique's 1 nm probing depth. An in-situ Ar ion gun at 800 eV is used to mill off the top Au layer before imaging and to clean the surface of depolarizing contaminants. Auger electron spectroscopy is then used to confirm the composition of the surface. Once the Au layer is removed, a Fe layer of 0.6 nm is deposited over the Py via in-situ molecular beam epitaxy. The Fe layer exchange couples to the Py and provides a surface material with an inherently higher secondary electron spin polarization compared to bare Py. Field pulses are applied in-plane at arbitrary directions with an electromagnet in a separate chamber at 10^{-6} Pa without breaking vacuum.

To nucleate domain walls in the nanowire array and initialize the triangles, a field of $\boldsymbol{B}_n$ = 110 ± 20 mT was applied at -10° from the *–x* direction and ramped to zero over 20 s. This was done to ensure that the domain walls are slightly offset in the *–y* direction in the nucleation structure and the triangles have a remanent buckle state in the *–x* direction. The large magnitude of $\boldsymbol{B}_n$ is greater than the typical field required to saturate these nanowire structures. Propagation fields of 7.5 ± 2 mT and 10 ± 2 mT were applied to the array during separate experiments. The domain wall structure was imaged before applying $\boldsymbol{B}_p$ and also in instances when the domain wall become pinned.

The micrographs of magnetization in Fig. 4a demonstrate SEMPA's ability to image domain wall structure and aid in identifying the nanowire geometry and field strength that results in reliable behavior. The contrast in Fig. 4a shows the transverse magnetization, M_y. Head-to-head domain walls in Fig. 4a(i) and 4a(ii) show characteristic wedge-shaped transverse configurations of downward and upward chirality, respectively, from nanowires of 100 nm width. The domain wall behavior in 150 nm wide nanowires proved to be less reliable than in 100 nm nanowires as evidenced by phase transformations to vortex structures after application of the propagation field, as seen in Fig. 4a(iii). Nanowires of 100 nm width appeared much more reliable with no chirality reversals ever being imaged with SEMPA. A domain wall pinned just before a triangle pair is seen to maintain its downward chirality in Fig. 4a(iv). Note that the rounded triangle tips in the magnetization images of Fig. 4a(iii) and 4a(iv) don't indicate actual fabrication results, but rather the resolution of the magnetization data. An example of typical fabrication results is also shown in the inset of Fig. 4c.

A 100 nm nanowire system with triangles having a base length of 1.2 μm and an aspect ratio of 1.317 with a spacing of 40 nm was found to have the correct behavior for both its element pairs. The initialized state after applying $\boldsymbol{B}_n$ is shown in the SEMPA image in Fig. 4b. All four triangles are seen to be in the $-x$ buckle state. The inset of Fig. 4b shows detail of SEMPA data from the domain wall nucleated in the curved structure. It is found to be pinned in the lower half of the nucleation structure, ready to be injected into the nanowire. The final result after applying $\boldsymbol{B}_p$ = 7.5 mT is shown in Fig. 4c and typifies a correct result with the bottom triangles in the $+x$ buckle state. While the boundaries of the coloring in Fig. 4b and 4c suggest

the domain wall tips are touching the nanowire, this was confirmed not to be the case as seen in the SEM micrograph in the inset of Fig. 4c.

Experimental results for 100 nm nanowires and a field of $\boldsymbol{B}_p$ = 7.5 mT had the overall trend of favoring a slightly lower aspect ratio for small base lengths compared to the simulations. Correct experimental results are noted by the green stars over the phase diagram in Fig. 3b(i). Additionally, all incorrect experimental results are noted by the black stars in the phase diagrams in Fig. 3b. The both-switch and no-switch experimental results, not shown, have the trend of favoring low aspect ratio and high aspect ratio, respectively. There are five geometries producing correct results compared to one producing an incorrect result. At a base length of 1.2 μm, two of the aspect ratios producing correct results track closely to the correct simulation result at a = 1.406. The three others, representing smaller elements, lie at an aspect ratio of 1.155, less than predicted by the modeling, which is possible if element variations due to fabrication raise the intrinsic coercivity.

For a field of $\boldsymbol{B}_p$ = 10 mT (stars overlaid in Fig. 3b(ii)), experimental results showed an increase of incorrect results, suggesting that a higher error rate occurs for higher bias fields. This is due possibly to an increased likelihood of Walker breakdown. Correct experimental results lie close to the phase space predicted by the modeling and again skew towards larger scale elements. This is likely a result of fabrication defects dominating the behavior of the smaller sized elements. For elements spaced at 70 nm and 100 nm, no geometry in the array produced a correct result, indicating that the domain wall stray field is not strong enough at these spacings and giving further evidence that the correct experimental results are indeed domain wall-assisted.

The experiments also provided evidence that stray field from a domain wall is necessary in switching an element and that elements don't merely switch spontaneously from the bias field. For example, in one case, a domain wall was pinned in the nucleation structure and never propagated through the nanowire. In that case (b = 900 nm and a = 1.406), the phase diagram in Fig. 3b(i) predicted a correct result, but since the domain wall did not propagate, the triangle pairs maintained a no-switch result. However, results from pinning in this array were minimal.

To test the repeatability of a geometry identified with a correct result, the magnetization was reset to its initialized condition and a propagation field of 10 mT was applied 11 separate times. The system studied had two triangle pairs with a geometry of b = 900 nm, a = 1.406, and s = 40 nm. This is the geometry noted as being correct for both simulation and experimental results in Fig. 3b(ii). For the first element pair, the final result was correct seven times and a no-switch four times. For the second element pair, the final result was correct six times, a no-switch two times, and incorrect three times. While correct results were produced a majority of the time for each element pair, the no-switch results indicate that this may not be the optimum design and spacing for this system. The incorrect results may reveal Walker breakdown behavior, especially since they occurred in the second element pair, 3.4 µm away from the first element pair. E. R. Lewis et al. discuss the fidelity length[33] of a field-driven domain wall propagating through a nanowire as being the minimum distance over which the domain wall may experience a structural change. A field of 10 mT may have a fidelity length as low as 350 nm, which increases the likelihood of a chirality reversal occurring before the domain wall reaches the first triangle pair and especially before it reaches the second. The minimum

propagation field may be lowered, and thus the fidelity length raised, by increasing the radius of curvature of the nucleation structure[32].

Furthermore, during the repeatability experiments described above, for a geometry initially showing no-switch behavior (b = 600 nm, a = 1.406, and s = 40 nm), a no-switch result occurred 11 out of 11 times for each triangle pair. For a geometry initially showing both-switch behavior (b =1.2 µm, a = 1.406, and s = 40 nm), a both-switch result occurred 11 out of 11 times for each triangle pair.

V. CONCLUSION

In summary, an element design for locally sensing and storing data on transverse domain wall chirality was presented. These elements may be used in magnetic logic systems that use domain wall chirality as the binary state variable. Furthermore, they may be useful in nanowire systems where, through internal or inter-domain wall interactions, chirality affects the error rate of the system. Triangle shape GMR elements placed beside the nanowire detect the chirality through the transverse domain wall stray field asymmetry. In the presence of a strong stray field on just one side of the domain wall and a globally applied longitudinal bias field, the initial longitudinal magnetization of the element undergoes a reversal. This reversal originates as a rotation of spins at the tip of the triangle as it interacts with the stray field. The sign of the longitudinal component is conserved in the remanent state due to shape anisotropy. This allows data to be stored and the measurement pulses to be applied in zero field conditions. This also allows experimental systems to be characterized with SEMPA, which was used to compare results to designs predicted by micromagnetic modeling. Using a pair of elements instead of a single one allows the characterization of not just chirality, but also whether the

elements may have switched spontaneously or via the passage of a domain wall. Pinning was not found to be a major concern.

The successful design optimization of the elements, especially the aspect ratio, relies heavily on the applied bias field. Fields of 7.5 mT and 10 mT were used to simultaneously actuate domain wall motion and bias the sense elements. Correct detection of domain wall chirality occurred at aspect ratios near 1.4. The spacing was also found to be an important factor, and detection of domain walls was not observed at spacings ≥ 70 nm. At a spacing of 40 nm, correct results occurred around the aspect ratio by the simulations. While a spacing of 10 nm was not characterized in experimental results, a closer spacing was found to widen the design space, as seen in phase diagrams produced by the simulations. Overall size, and therefore scalability, was found to be limited to base lengths greater than 300 nm to allow shape anisotropy to dominate the magnetization orientation. However, smaller structures are preferred for faster element switching. While the triangle design was not optimized for repeatability in experiments, a design of triangles capable of producing correct chirality detection was found to produce the expected result a majority of the time from 11 iterations of the experiment. Switching errors in the experimental systems are likely due to variations in the magnetic orientation caused by expected fabrication defects and slight deviations in the applied field directions.

Switching errors manifested as an incorrect result may be the result of coercivity variations or an actual measurement of Walker breakdown causing a chirality reversal. For implementation in a logic system, it would be beneficial to actuate the system through an

alternative energy source other than an applied field, not only to reduce effects of Walker breakdown, but also to reduce design limitations and overall power requirements. Domain wall propagation via spin transfer torque is possible, but changes in domain wall structure and pinning on defects would still need to be addressed. In such a system, a separate bias would need to be applied to the triangle sense elements. Strain or charge-mediated control of magnetization through coupling to a ferroelectric underlayer is a technology that may be explored. With a high enough biasing force, a domain wall fan-out structure may be demonstrated without requiring a physical wire split by attaching a nanowire to a sense element. While the ability to detect domain wall stray field and structure was demonstrated for an in-plane magnetized system, this concept may also be extended to out-of-plane magnetized systems.

ACKNOWLEDGEMENTS

We would like to acknowledge the National Research Council Research Associateship Programs and the NIST-CNST/University of Maryland Nanocenter Cooperative Agreement. We are also grateful to R. D. McMichael for very useful discussions.

REFERENCES

[1]D. A. Allwood, G. Xiong, C. C. Faulkner, D. Atkinson, D. Petit, and R. P. Cowburn, *Science* **309**, 1688 (2005).

[2]R. P. Cowburn and M. E. Welland, *Science* **287**, 1466 (2000).

[3]A. Imre, G. Csaba, L. Ji, A. Orlov, G. H. Bernstein, and W. Porod, *Science* **311**, 205 (2006).

[4]Stuart S. P. Parkin, Masamitsu Hayashi, Luc Thomas, *Science* **320**, 190 (2008).

[5]D. Atkinson, D. S. Eastwood, and L. K. Bogart, *Appl. Phys. Lett.* **92**, 022510 (2008).

[6]D. A. Allwood, Gang Xiong, and R. P. Cowburn, *Appl. Phys. Lett.* **89**, 102504 (2006).

[7]G. Csaba, P. Lugli, and W. Porod, *4th IEEE Conference on Nanotechnology*, 346 (2004).

[8]S. R. Bowden and U. J. Gibson, *IEEE Trans. Magn.* **45**, 5326 (2009).

[9]G. Csaba, J. Kiermaier, M. Becherer, S. Breitkreutz, X. Ju, P. Lugli, D. Schmitt-Landsiedel, and W. Porod, *J. Appl. Phys.* **111**, 07E337 (2012).

[10]E. Varga, G. Csaba, G. H. Bernstein, and W. Porod, *IEEE Trans. Magn.* **48**, 3563 (2012).

[11]L. O'Brien, A. Beguivin, A. Fernandez-Pacheco, D. Petit, D. E. Read, and R. P. Cowburn, *Appl. Phys. Lett.* **101**, 062415 (2012).

[12]M. Laufenberg, D. Bedau, H. Ehrke, M. Kläui, and U. Rüdiger, *Appl. Phys. Lett.* **88**, 212510 (2006).

[13]R. D. McMichael and M. J. Donahue, *IEEE Trans. Magn.* **33**, 4167 (1997).

[14]A. Kunz, *Appl. Phys. Lett.* **94**, 132502 (2009).

[15]Y. Jang, S. R. Bowden, M. Mascaro, J. Unguris, and C. A. Ross, *Appl. Phys. Lett.* **100**, 062407 (2012).

[16]L. O'Brien, D. Petit, H. T. Zeng, E. R. Lewis, J. Sampaio, A. V. Jausovec, D. E. Read, and R. P. Cowburn, *Phys. Rev. Lett.* **103**, 077206 (2009).

[17]T. J. Hayward, M. T. Bryan, P. W. Fry, P. M. Fundi, M. R. J. Gibbs, M.-Y. Im, P. Fischer, and D. A. Allwood, *Appl. Phys. Lett.* **96**, 052502 (2010).

[18]E. R. Lewis, D. Petit, L. Thevenard, A. V. Jausovec, L. O'Brien, D. E. Read, and R. P. Cowburn, *Appl. Phys. Lett.* **95**, 152505 (2009).

[19]Dorothée Petit, Ana-Vanessa Jausovec, Dan Read, and Russell P. Cowburn, *J. Appl. Phys.* **103**, 114307 (2008).

[20]M. A. Bashir, M. T. Bryan, D. A. Allwood, T. Schrefl, J. S. Claydon, G. Burnell, and C. H. Marrows, *J. Appl. Phys.* **110**, 123912 (2011).

[21]M. J. Donahue and D. G. Porter, OOMMF User's Guide, Version 1.0 Interagency Report NISTIR 6376, National Institute of Standards and Technology, Gaithersburg, MD (1999), http://math.nist.gov/oommf

[22]M. R. Scheinfein, J. Unguris, M. H. Kelley, D. T. Pierce, and R. J. Celotta, *Rev. Sci. Instrum.* **61**, 2501 (1990).

[23]L. Thevenard, H. T. Zeng, D. Petit, and R. P. Cowburn, *J. Appl. Phys.* **106**, 063902 (2009).

[24]L. Thevenard, H. T. Zeng, D. Petit, and R. P. Cowburn, *J. Magn. Magn. Mater.* **322**, 2152 (2010).

[25]S. Yakata, M. Miyata, S. Nonoguchi, H. Wada, and T. Kimura, *Appl. Phys. Lett.* **97**, 222503 (2010).

[26]M. Miyata, K. Kiseki, S. Yakata, H. Wada, and T. Kimura, *J. Appl. Phys.* **111**, 07B902 (2012).

[27]Saturation magnetization M_s = 800 x 10^3 A/m and exchange stiffness A = 13 x 10^{-12} J/m.

[28]Exchange stiffness A = 13 x 10^{-12} J/m, damping parameter α = 0.01, M_s = 800 x 10^3 A/m, and cell size = 10 nm.

[29]M_s = 860 x 10^3 A/m, α = 0.5, A = 13 x 10^{-12} J/m, and cell size = 12 nm.

[30]M_s = 800 x 10^3 A/m, A = 13 x 10^{-12} J/m, cell size = 10 nm, stopping criteria: $|\boldsymbol{m} \times \boldsymbol{H}_{\text{eff}} \times \boldsymbol{m}|$ = 1 A/m, $\boldsymbol{m}$ is the unit spin magnetization and $\boldsymbol{H}_{\text{eff}}$ is the effective internal field.

[31]α = 0.01 and minimum d$\boldsymbol{m}$/dt = 0.1 degrees per nanosecond.

[32]N. L. Schryer and L. R. Walker, *J. Appl. Phys.* **45**, 5406 (1974).

[33]E. R. Lewis, D. Petit, A.-V. Jausovec, L. O'Brien, D. E. Read, H. T. Zeng, and R. P. Cowburn, *Phys. Rev. Lett.* **102**, 057209 (2009).

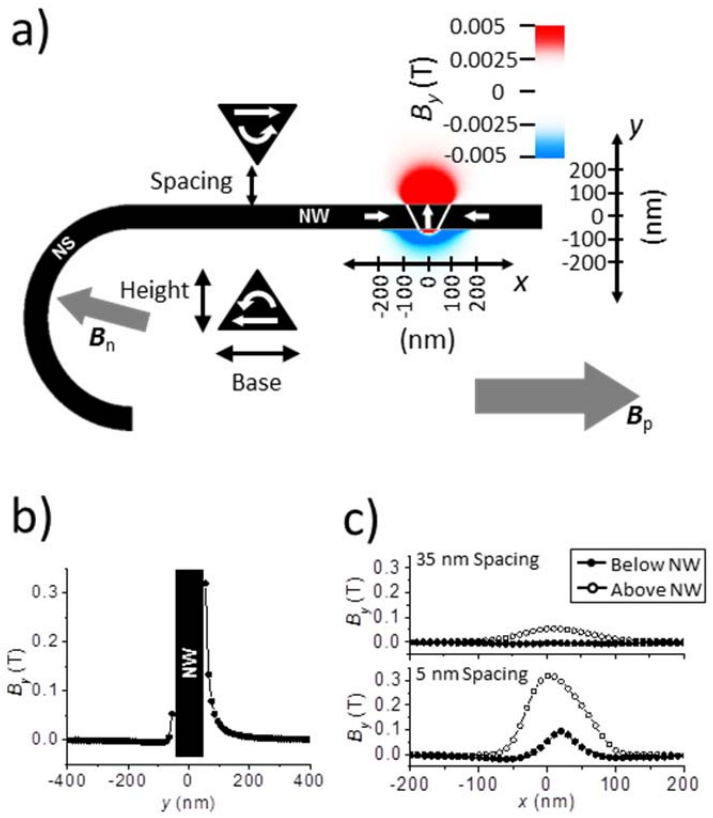

Fig. 1. (a) Composite schematic and OOMMF field calculation showing the relevant parameters of Py triangle size and placement beside a Py nanowire (NW) and curved nucleation structure (NS). Shown by the color scale is the calculation of the transverse component of the stray field, B_y, emitted by a transverse domain wall oriented in the $+y$ direction. White arrows show the end result magnetization after a domain wall traverses the nanowire from left to right with field $\boldsymbol{B}_p$ after the triangles and nanowire have been biased by the domain wall nucleation field, $\boldsymbol{B}_n$. (b) Transverse line scan that bisects the OOMMF-calculated transverse field, B_y. (c) Horizontal line scans of B_y above and below the nanowire at 35 nm spacing (upper panel) and 5 nm spacing (lower panel).

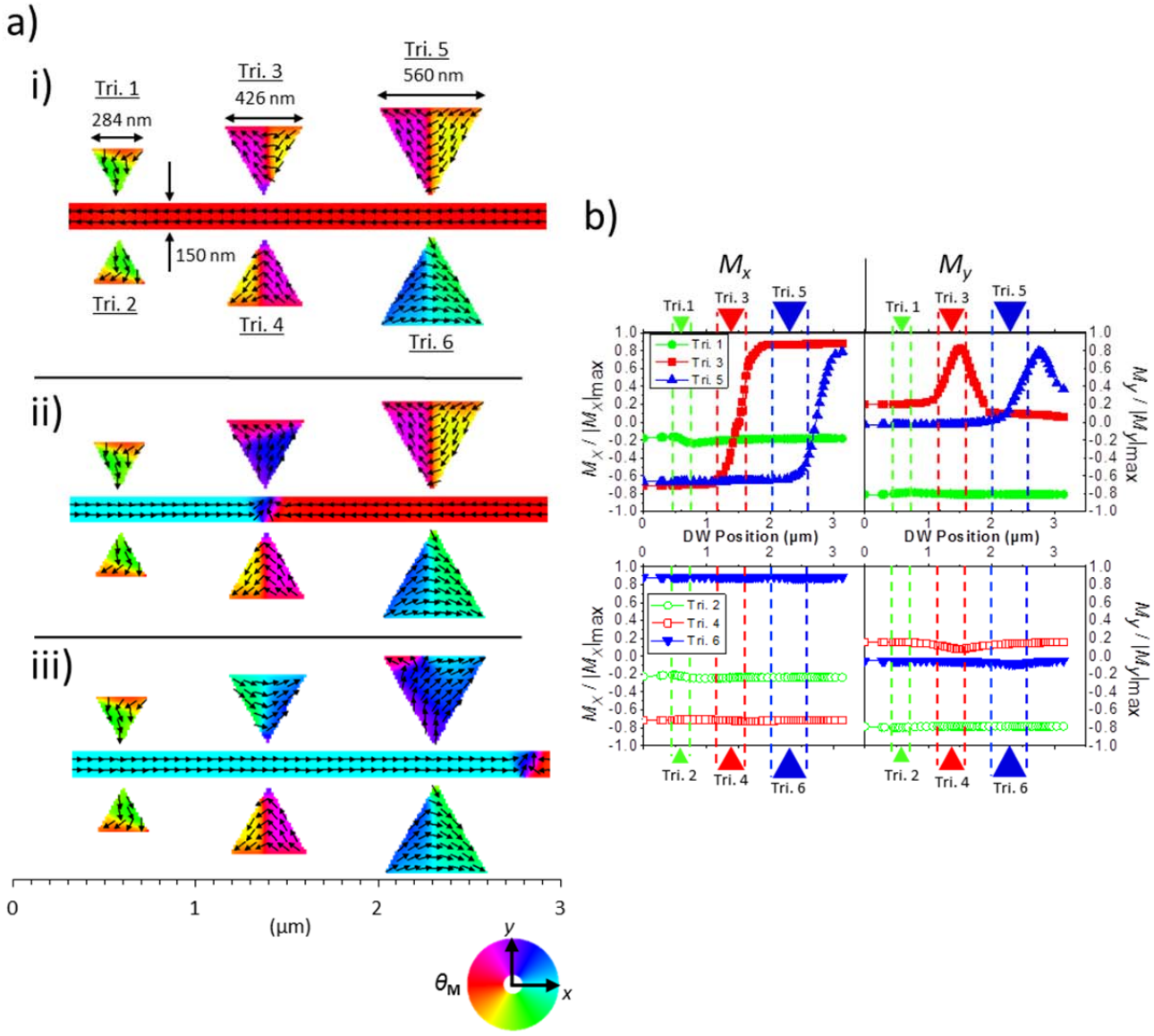

Fig. 2. OOMMF results showing scaling effects for Py triangle element switching in the presence of a moving transverse domain wall (DW) in a 150 nm wide nanowire and a bias field of 14.5 mT applied in the $+x$ direction. With a constant aspect ratio of 1.163 and thickness of 10 nm, three triangle pairs with base lengths of 284 nm (triangles 1 and 2), 426 nm (triangles 3 and 4), and 560 nm (triangles 5 and 6) are examined. Three frames of the simulation are shown in (a), with the domain wall positioned before entering the vicinity of the triangles, (i), between the middle pair, (ii), and exiting the domain wall, (iii). Color indicates magnetization direction as shown by the color wheel. For each element the total longitudinal magnetization, M_x, and transverse magnetization, M_y, is plotted against domain wall position in (b). The upper triangle responses are shown in the top row, and the lower ones in the bottom row. The value $M_{x\,(y)}/|M_{x\,(y)}|_{max}$ for an individual element is calculated as the sum total of the longitudinal (transverse) component of all cells in the element divided by the sum total of each cell's magnetization in the case where the element is completely magnetized in the $+x$ ($+y$) direction.

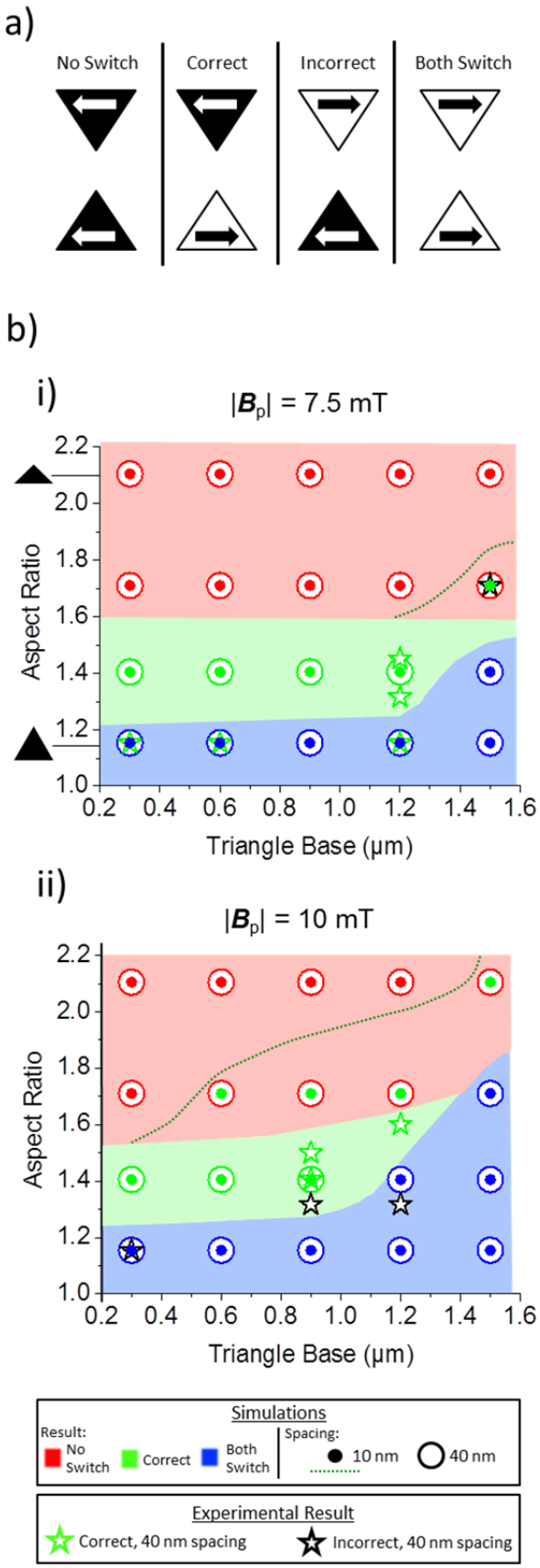
a)
No Switch
Correct
Incorrect
Both Switch
b)
i)
|B_p| = 7.5 mT
Aspect Ratio
Triangle Base (μm)
ii)
|B_p| = 10 mT
Aspect Ratio
Triangle Base (μm)
Simulations
Result:
No Switch
Correct
Both Switch
Spacing:
10 nm
40 nm
Experimental Result
Correct, 40 nm spacing
Incorrect, 40 nm spacing

Fig. 3. Phase diagram results of Py triangle switching behavior after a transverse domain wall with downward chirality propagates through a 10 nm thick, 100 nm wide Py nanowire. The possible outcomes in (a) are plotted in the phase diagrams of (b), which describe results from varying values of spacing, aspect ratio, and base length. Results are shown after applying 7.5 mT (i) and 10 mT (ii) bias fields. Simulation data points are represented by filled dots (10 nm spacing) and open circles (40 nm spacing). Colored shading corresponds to possible phase boundaries for the 40 nm spacing simulation results. The green dotted lines indicate the extension of the "correct" phase for the 10 nm spacing simulation results. "Correct" and "incorrect" data points from the experimental results are represented by the green and black stars, respectively.

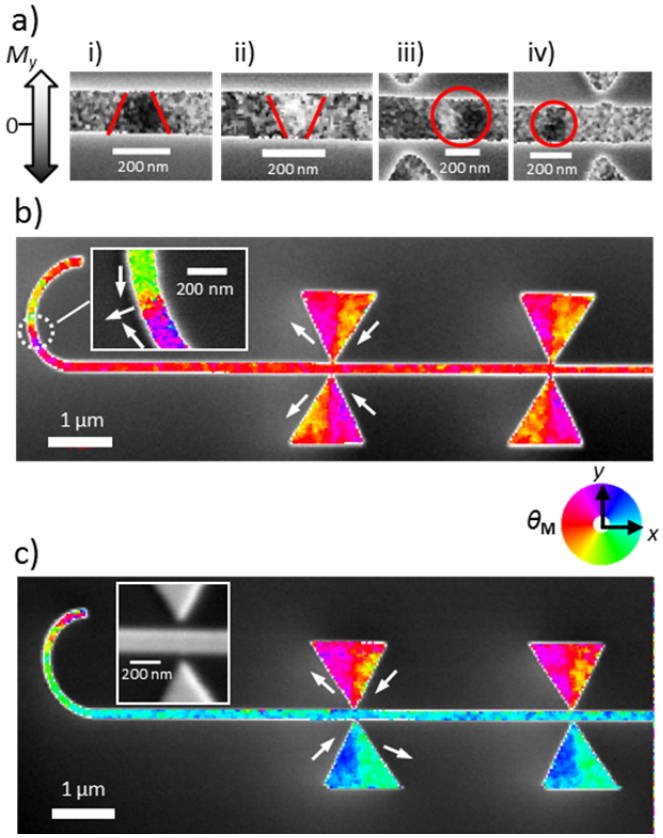

Fig. 4. SEMPA micrographs of domain walls with transverse magnetization, M_y, contrast are shown in (a). A downward (i) and upward (ii) transverse domain wall occur in a Py nanowire of 100 nm width and injected using a r = 600 nm nucleation structure. A structural phase transformation from a transverse domain wall to a vortex domain wall occurs in Py nanowires of 150 nm width (iii). A pinned transverse domain wall (iv) has the same initial chirality. Red lines in (a) indicate approximate boundaries or locations of the domain walls. A 100 nm wide nanowire, 10 nm thick system with triangle pairs having b = 1.2 µm, a = 1.317, and s = 40 nm produced the correct result after applying a propagation field of $\boldsymbol{B}_p$ = 7.5 mT. SEMPA images before (b) and after (c) propagating the domain wall indicate the magnetization angle, θ_M (see color wheel for reference). White arrows in (b) and (c) indicate the approximate overall magnetization direction of the nearby Py pattern. The inset of (b) shows detail of the nucleated domain wall. The inset of (c) shows an SEM micrograph of typical fabrication results. The skewing seen in (b) is a result of image drift and is not real.